Microwave Imaging for Lung Covid-19 Infection Detection through Huygens Principle

B. Khalesi[1, 2, 3], **B. Khalid**[1], **N. Ghavami**[2, 3],
S. Dudley[1], **M. Ghavami**[1], **and G. Tiberi**[1, 2, 3]

[1]School of Engineering, London South Bank University, London, UK
[2]Umbria Bioengineering Technologies, Perugia, Italy
[3]UBT UK Division, London, UK

Abstract— This paper aims to show the capability of the Huygens Principle-based microwave imaging for use in Lung COVID-19 infection detection. Frequency-domain measurements have been performed in an anechoic chamber using two Microstrip antennas operating at frequency range of 1 to 5 GHz, in a multi-bistatic fashion, employing dedicated phantoms that mimic the dimensions and the dielectric properties of a human torso, containing a target mimicking an infection. A Multi-layered elliptically-shaped torso-mimicking phantom having the circumference of 82 cm has been constructed; the external layer mimics the dielectric properties of a combination of muscle, fat and rib bone tissues, the inner layer mimics the dielectric properties of lung (inflated). A cylindrically-shaped tube of water has been positioned inside the inner layer to dielectrically mimic the infection. The S_{21} signals have been used for image reconstruction (after removing artifacts), obtaining detection with a signal to clutter ratio of 7 dB. Our results confirm that Huygens based technique can be successfully used for lung infection detection even if antennas and phantom are in free space, i.e., no coupling liquid is required.

1. INTRODUCTION

COVID-19, which emerged in late 2019, has now become a worldwide pandemic. COVID-19 lung lesions may manifest with chest CT imaging abnormalities, even in asymptomatic patients, with evolution to diffuse bilateral ground-glass opacities [1]. However, it is not recommended to use CT as a routine screening modality because it should be reserved for hospitalized and symptomatic patients. Moreover, although CT is important for the tracking of the treatment procedure of COVID-19 infection [2], the accumulation of ionizing radiation may represent a concern when using this technique for monitoring.

Microwave imaging has attracted growing attention, especially for its applicability towards breast cancer detection, motivated by the significant contrast in the dielectric properties at microwave frequencies (1–10 GHz) between normal and malignant tissues [3]. Recently, microwave imaging has also been applied for brain stroke classification, bone imaging and lung cancer detection [4, 5]. Specifically, in [4], the authors introduced a three-dimensional electromagnetic torso scanner that operates between 0.83 and 1.9 GHz. In [4] and [5] it is reported that the relative permittivity and conductivity of cancerous tissues are up to 3 times and 2 times larger than normal tissues, respectively.

Since COVID-19 infection leads to ground-glass opacities in the lungs as shown in [2], such opacities imply a contrast in dielectric properties with respect to the surrounding normal tissues [6]; it follows that microwave imaging could detect such opacities, which are larger in size than lung cancers.

In general, current research in microwave imaging can be divided mainly into tomography and linear scattering techniques. Among linear scattering techniques, the Huygens Principle (HP) based technique allows to detect dielectric inhomogeneities in frequency domain [7]. Specifically, using HP to forward propagate the UWB signals collected outside the investigation domain permits the capture of contrast, i.e., the extent to which different tissues, or different condition of tissues, can be discriminated in the final image. In addition, HP requires a very simple hardware set-up, i.e., one transmitting antenna and one receiving antenna, coupled through a vector network analyzer (VNA), which rotate around the object to collect the signal in a multi-bistatic fashion. Up to now, HP has been used for breast, bone, and brain imaging.

The aim of this paper is to assess the capability of the proposed HP procedure in detecting Lung COVID-19 infection through measurements inside an anechoic chamber employing dedicated

phantoms that mimic the dimensions and the dielectric properties of a human torso, containing a target mimicking an infection. In order to detect the Lung COVID-19 infection inside a human torso phantom, frequency-domain measurements have been performed in an anechoic chamber using a VNA arrangement to obtain the transfer function ($S21$) between two microstrip antennas operating between 1 and 5 GHz in a multi-bistatic fashion. This band has shown to be optimal for lung imaging [4]; in addition, in [7] it is clearly highlighted that a large bandwidth can enhance performance in lesion detection. Next, $S21$ signals have been used for image reconstruction, removing artifacts via a rotation subtraction procedure.

2. MATERIALS AND METHODS

2.1. Phantom Reconstruction

This section details the design and fabrication process of human torso phantom by considering the relative permittivity and conductivity with the aim of performing microwave imaging experiments in the frequency range of 1 to 5 GHz to validate the efficiency of the HP imaging algorithm in detecting the Lung COVID-19 infection. Our torso mimicking phantom is comprised of 2 layers in elliptical shape. The external layer has an oval shape with axes of 31 cm and 20 cm (and height of 25 cm); thus, its circumference of 82 cm may be representative of a small-size chest circumference. The oval-shaped internal layer has axes of 27 cm and 14 cm (and height of 25 cm). The small cylindrically shaped plastic tube having 15 ml volume has been mounted on the inner layer's wall, as shown in Fig. 1.

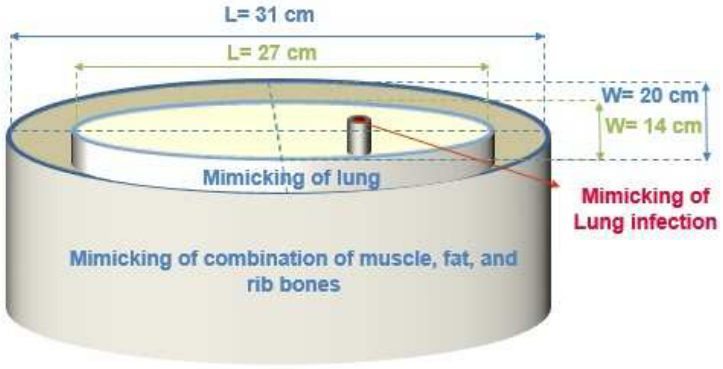

Figure 1: Design of lung COVID-19 infection phantom.

The external layer mimics a combination of muscle, fat and rib bone tissues; the internal layer mimics the lung tissue, and the cylindrical tube simulates the lung infection. Table 1 displays the dielectric properties of real tissues, derived from [8, 9].

Table 1: Relative permittivity and conductivity at a frequency of 2 GHz [4, 8, 9].

Different layers of human torso phantom	Relative Permittivity	Conductivity (S/m)
Fat	5	0.08
Muscle	50	1.45
Rib bone	12	0.3
Lung (inflated)	20	0.1
Lung infection	60	2.5

The phantom fabrication has been performed through the following steps. The small oval-shaped container has been filled up with the mixture of 90% glycerol and 10% water having relative permittivity equal to 15 and conductivity equal to 0.2 S/m at 2 GHz; thus, it may be considered as mimicking the dielectric properties of the lung (inflated) [10]. The small oval-shaped container has been positioned inside the external layer. Next, a dedicated oil (TLe11.5C.045, purchased from the ZMT Zurich MedTech Company [11]) with relative permittivity of 7 and conductivity of 0.3 S/m at 2 GHz has been used; it mimics a combination mixture of muscle, fat and rib bone tissues and has been poured to completely fill the remaining space surrounding the lung layer. Subsequently,

the small cylindrically shaped plastic tube has been filled with tap water as the lung infection-mimicking material and then positioned inside the internal wall [4, 6]. Fig. 2 shows the fabricated human torso phantom.

Figure 2: The lung COVID-19 infection fabricated phantom.

As can be found from Table 1, the fabrication procedure for each layer of phantom has been performed by considering the similarity of the dielectric properties (permittivity and conductivity) of the layers with the tissues to be mimicked. It is also important to point out that, the stability of the used materials and the geometric dimension similarity between each layer and the realistic scenarios have been observed in the fabrication procedure.

2.2. Experimental Configurations in an Anechoic Chamber

The frequency domain measurements have been performed inside the anechoic chamber using frequency range of 1–5 GHz. In order to acquire back scattered signals from the human torso phantom, the multi-bistatic configuration has been employed by using two different UWB antennas which are vertically polarized and omni-directional in the azimuth plane and have been placed in free space. Two UWB antennas have been connected to a VNA (model MS2028C, Anritsu) and have been used for transmitting and receiving the signals, after calibration. In a multi-bistatic fashion, one of the antennas is used as a transmitter while another is used as a receiver and rotates around the object to collect the $S21$ scattered signals in different directions.

The multi-layered infected lung phantom has been placed in the center of the rotatable table having a distance of 21 cm and 30 cm away from the receiver and transmitter antennas, respectively. The measurement procedure has been performed for two different transmitting positions displaced

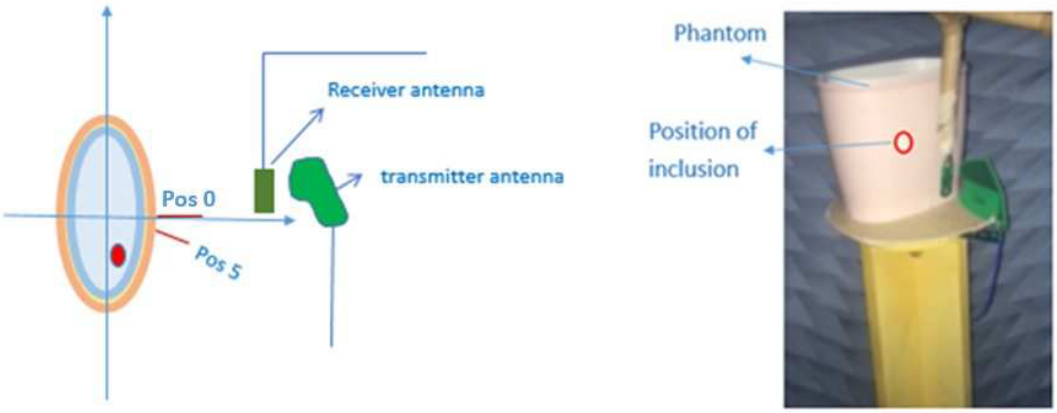

Figure 3: (a) Pictorial view of the measurement set up; (b) Position of the torso phantom inside the anechoic chamber. The phantom was placed on the centre of a rotatable table. The external planar UWB horn antenna (310C Next-RF) is the transmitter, and the internal UWB antenna (PulsON P200) is the receiver.

at 0° and 5°. For each transmitting position, the $S21$ signal has been recorded for 60 receiving points (NPT = 60) through rotating the receiver antenna and collecting the signals every 6° over the frequency range of 1 to 5 GHz, using a frequency sample spacing of 5 MHz. The experiment has been repeated for the "healthy" scenario which is the torso phantom with no lung-infection layer. Figs. 3(a) and 3(b), show the pictorial view of the measurement setup and the position of the multi-layered torso phantom inside the anechoic chamber, respectively.

2.3. Description of the HP-based Imaging Procedure

The Huygens Principle imaging procedure has been applied to the measured complex $S21$ of the VNA to reconstruct the images [12]. Specifically, the torso phantom which has been placed in free space, is exposed to the signal emitted by the transmitter antenna located at the position TX_m. The $S21$ signals has been collected at the point $\mathrm{RX}_{np} \equiv (r_0, \phi_{np}) \equiv \vec{\rho}_{np}$ through rotating the receiving antenna around the phantom displaced along a circular surface having radius r_0 (see Fig. 4) which can be expressed as $S21_{\mathrm{TX}_m}|_{\mathrm{RX}_{np}} = S21_{np,\mathrm{TX}_m}$. The position of the receiving antenna is shown by RX_{np}, np is the number of receiving position that varies from 1 to N_{PT} and subscript m represents the transmitting positions with $m = 1, 2$. The two transmitting positions displaced 5° apart from each other, have been synthesized by accurately rotating the phantom instead of displacing the transmitting antenna positions.

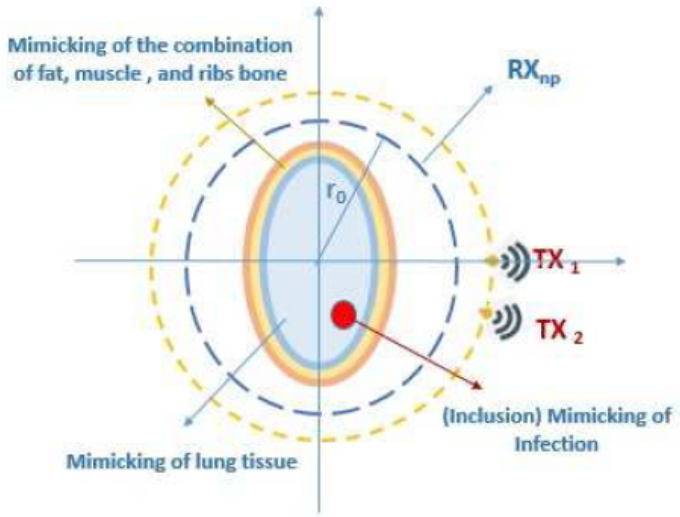

Figure 4: Pictorial view of the measurements.

By referring to Huygens Principle, we can write [12]:

$$E^{\mathrm{rcstr}}_{\mathrm{HP,2D}}(\rho, \phi; \mathrm{TX}_m; f) = \Delta_s \sum_{np=1}^{N_{PT}} S21^{\mathrm{known}}_{np,\mathrm{TX}_m} G\left(k_1 |\overrightarrow{\rho}_{np} - \overrightarrow{\rho}|\right) \tag{1}$$

In Equation (1) the observation point is shown by $(\rho, \phi) \equiv \overrightarrow{\rho}$, while the spatial sampling and number of waves are presented by the parameters Δ_s and k_1 respectively. In $E^{\mathrm{rcstr}}_{\mathrm{HP,2D}}$, two strings "rcstr" and "HP" indicate the reconstructed internal field, and the employed Huygens principle-based procedure, respectively. $G(k_1|\overrightarrow{\rho}_{np} - \overrightarrow{\rho}|)$ represent the Green's function.

Subsequently, the intensity of the final image I can be defined by assumption of using N_F frequencies through Equation (2), i.e., by summing incoherently all the solutions.

$$I(\rho, \phi; \mathrm{TX}_m) = \sum_{i=1}^{N_F} \left| E^{\mathrm{rcstr}}_{\mathrm{HP}}(\rho, \phi; \mathrm{TX}_m; f_i) \right|^2 \tag{2}$$

Since the artifact, i.e., the image of the transmitter or reflections of the layers, might mask the region of the interest, the signal pre-processing method should be applied to suppress artifacts. In this paper the appropriate artifact removal method has been performed on the measured data with the aim of eliminating the artifacts and achieving the accurate detection. For this purpose, the

following two distinct methods have been employed here to remove the artifact; (i) the rotation subtraction between $S21$ obtained using two slightly displaced transmitting positions (5° apart), (ii) the "ideal" artifact removal method using subtraction between obtained data of a "healthy" torso phantom and the data of torso phantom having lung infection.

2.4. Image Quantification

In this paper, image quantification has been presented to investigate the performance of the imaging procedure through introducing the calculation of a metric which is called signal to clutter ratio (SCR). In fact, the ratio between maximum intensity evaluated in the region of the lesion divided by the maximum intensity outside the region of the lesion is defined as a SCR [13].

3. RESULTS AND DISCUSSION

The obtained microwave images using the HP-based imaging procedure are shown in Figs. 5 and 6. In the presented images, the light blue ellipse region represents the torso phantom, while the red circle region indicates the true area of the lung infection. Moreover, it is important to point out that all the images shown here were normalized and adjusted, forcing the intensity values below 0.5 to zero.

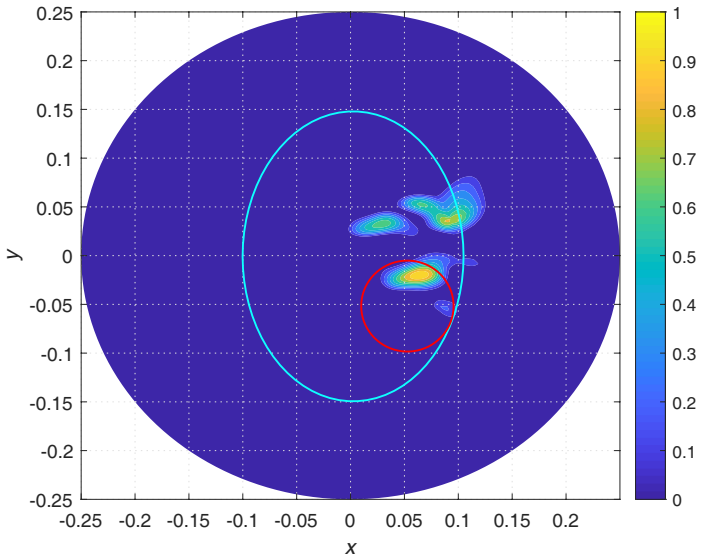

Figure 5: Microwave image of the human torso phantom employing frequency range of 1–5 GHz after performing rotation subtraction artifact removal procedure using the difference between measurements obtained with transmitting positions 0° and 5°; The light blue line indicates the phantom ellipse in ext (external layer), while the red line represents the actual inclusion position; Images are obtained following normalization to their correspondent maximum values and forcing to zero the intensity values below 0.5 (x and y axes are given in meters).

Figure 5 shows the obtained microwave image (normalised to the maximum) of the phantom when employing the rotation subtraction artifact removal procedure between $S21$ obtained using transmitting positions 0° and 5°. Although the residual clutter can be seen in Fig. 5, however, the inclusion is clearly detectable in the correct position.

Figure 6 refers to the obtained microwave image of the human torso phantom when performing "ideal" artifact removal procedure which is using difference between obtained data of a healthy torso phantom and the data of torso phantom having lung infection. As Fig. 6 depicts, the inclusion is visible in its correct position without any residual clutter. Moreover, the resulting outcome from performing artifact removal method using the difference between obtained data of a healthy torso phantom and unhealthy torso phantom confirms the previous results.

Accordingly, the capability of the imaging procedure for lung infection detection can be confirmed through a visual inspection. Moreover, image quantification has been performed by calculating SCR. The SCR value calculated when applying rotation subtraction artifact removal reached 4.65 dB, while this value increases to 7 dB when performing "ideal" artifact removal procedure.

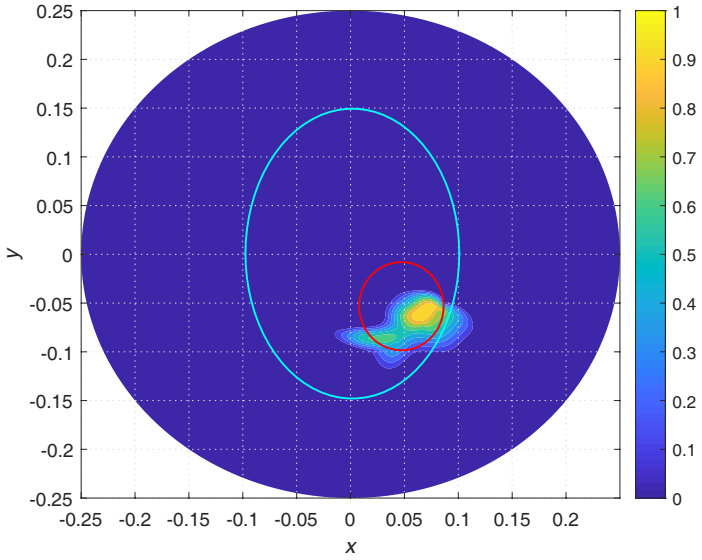

Figure 6: Microwave image of the human torso phantom employing frequency range of 1–5 GHz; after performing "ideal" artifact removal procedure; using the difference between obtained data of a healthy torso phantom and the data of torso phantom having lung infection. The light blue line indicates the phantom ellipse in ext (external layer), while the red line represents the actual inclusion position. Images are obtained following normalization to their correspondent maximum values and forcing to zero the intensity values below 0.5 (x and y axes are given in meters).

4. CONCLUSIONS

This paper presented the results of a microwave imaging procedure based on Huygens principle for Lung COVID-19 infection detection. The results were derived from measurements on a human torso phantom inside the anechoic chamber using two Microstrip antennas operating between 1 and 5 GHz. The identification of the lung infection has been achieved after employing artifact removal procedure to eliminate the artifact, i.e., the images of the transmitter or the reflection of first layer. The rotation subtraction artifact removal method has been applied using two slightly displaced transmitting positions, and also using subtraction between obtained data of a healthy torso phantom and the data of torso phantom having lung infection, to suppress the artifact and preventing the masking of the inclusion region. The quantification of the microwave images have been calculated using SCR, achieving 7 dB.

HP can also be used if antennas and phantom are in free space, i.e., no coupling liquid is required; in addition, HP does not require any knowledge of antennas' responses. HP based technique can be easily integrated in a device which will be cost-effective, easy to build, use and integrate in a dedicated detection space, allowing remote pre-hospital examinations and monitoring of Lung COVID-19 infection.

ACKNOWLEDGMENT

This project has received funding from the European Union's Horizon 2020 research and innovation program under grant agreements No.: 830265, 872752, 101017098.

REFERENCES

1. Huang, C., Y. Wang, X. Li, L. Ren, J. Zhao, et al., "Clinical features of patients infected with 2019 novel coronavirus in Wuhan, China," *The Lancet*, Vol. 395, No. 1023, 497–506, 2020.
2. Shi, H., X. Han, N. Jiang, Y. Cao, O. Alwalid, J. Gu, et al., "Radiological findings from 81 patients with COVID-19 pneumonia in Wuhan, China: A descriptive study," *The Lancet Infectious Diseases*, Vol. 20, No. 4, 425–434, 2020.
3. Byrne, D., *An Introduction to Microwave Imaging for Breast Cancer Detection*, 47–73, Springer International Publishing: Biological and Medical Physics, Biomedical Engineering, 2016.
4. Rezaeieh, S. A., A. Zamani, K. S. Bialkowski, and A. M. Abbosh, "Novel microwave torso scanner for thoracic fluid accumulation diagnosis and monitoring," *Scientific Reports*, Vol. 7, No. 1, 1–10, 2017.

5. Muhammad, S. N., M. Mohamad Isa, and F. Jamlos, "Review article of microwave imaging techniques and dielectric properties for lung tumor detection," *AIP Conference Proceedings*, Vol. 2203, No. 1, 020012, 2020.
6. Lin, X., Z. Gong, Y. Ding, Y. Chen, P. A. V. Sosa, and M. J. V. Sosa, "Feasibility study of detection of coronavirus disease 2019 with microwave medical imaging," *2021 15th European Conference on Antennas and Propagation (EuCAP)*, 1–4, Dusseldorf, Germany, March 2021.
7. Ghavami, N., G. Tiberi, D. J. Edwards, and A. Monorchio, "UWB microwave imaging of objects with canonical shape," *IEEE Transactions on Antennas and Propagation*, Vol. 60, No. 1, 231–239, 2012.
8. Hasgall, P. A., F. Di Gennaro, C. Baumgartner, E. Neufeld, B. Lloyd, M. C. Gosselin, et al., "IT'IS database for thermal and electromagnetic parameters of biological tissues, Version 4.0," *IT'IS*, 2018.
9. Gabriel, S., R. W. Lau, and C. Gabriel, "The dielectric properties of biological tissues: III. Parametric models for the dielectric spectrum of tissues," *Physics in Medicine & Biology*, Vol. 41, No. 11, 2271, 1996.
10. Meaney, P. M., C. J. Fox, S. D. Geimer, and K. D. Paulsen, "Electrical characterization of glycerin: Water mixtures: Implications for use as a coupling medium in microwave tomography," *IEEE Transactions on Microwave Theory and Techniques*, Vol. 65, No. 5, 1471–1478, 2017.
11. Zurich Med Tech. Available: https://zmt.swiss/validation-hw/tsm/tle5c-24-2450/ [Accessed: 26-10-2019].
12. Tiberi, G., N. Ghavami, D. J. Edwards, and A. Monorchio, "Ultrawideband microwave imaging of cylindrical objects with inclusions," *IET Microwaves, Antennas & Propagation*, Vol. 5, No. 12, 1440–1446, 2011.
13. Fear, E. C., X. Li, S. C. Hagness, and M. A. Stuchly, "Confocal microwave imaging for breast cancer detection: Localization of tumors in three dimensions," *IEEE Transactions on Biomedical Engineering*, Vol. 49, No. 8, 812–822, 2002.